

Bayesian Supervised Causal Clustering

Luwei Wang¹ Nazir Lone²
Sohan Seth¹

¹School of Informatics, University of Edinburgh, Edinburgh, UK

²Usher Institute, University of Edinburgh, Edinburgh, UK

Abstract

Finding patient subgroups with similar characteristics is crucial for personalized decision-making in various disciplines such as healthcare and policy evaluation. While most existing approaches rely on unsupervised clustering methods, there is a growing trend toward using supervised clustering methods that identify operationalizable subgroups in the context of a specific outcome of interest. We propose Bayesian Supervised Causal Clustering (BSCC), with *treatment effect as outcome* to guide the clustering process. BSCC identifies homogenous subgroups of individuals who are similar in their covariate profiles as well as their treatment effects. We evaluate BSCC on simulated datasets as well as real-world dataset from the third International Stroke Trial to assess the practical usefulness of the framework.

1 Introduction

Patient stratification, i.e., the identification of subgroups sharing clinical, molecular, or genetic characteristics, is a cornerstone of precision medicine and data-driven decision-making [Abdelnour et al., 2022]. By uncovering structured variation across high-dimensional population data, stratification enables clinicians to tailor treatments to specific groups, maximizing efficacy while minimizing adverse effects [Dubois et al., 2015]. Crucially, this approach addresses the challenge of Heterogeneity of Treatment Effects (HTE), where identical interventions yield divergent responses across subpopulations due to complex interactions between patient characteristics and treatment mechanisms [Thelen and Hennessy, 2025]. While Randomized Controlled Trials (RCTs) generally report Average Treatment Effects (ATE), such aggregate summaries often mask substantial variability in treatment response [Shehabi et al., 2021]. Ignoring this heterogeneity can lead to ineffective or even harmful clinical decisions: a modest overall benefit might obscure a large effect in a small, identifiable subgroup, or conversely, significant harm in another [Kravitz et al., 2004, Kent et al., 2018]. Consequently, identifying *clinically operationalizable* subgroups that are distinct not only in their observable features but also in their response to treatment is essential for guiding personalized therapeutic strategies.

Traditionally, unsupervised clustering methods such as Gaussian Mixture Models (GMM) [Fraley and Raftery, 2002] and Latent Class Analysis (LCA) [Collins and Lanza, 2010] have been the primary tools for data-driven patient stratification. These methods excel at uncovering hidden population structures by minimizing within-group variance in the covariate space [Murphy, 2012]. Approaches like k -means and LCA have been successfully applied to characterize disease phenotypes in conditions such as sepsis [Seymour et al., 2019], acute respiratory distress syndrome (ARDS) [Sinha et al., 2018], and hypertension [Guo et al., 2017]. However, a key limitation of unsupervised clustering is that the resulting subgroups are defined solely by covariate similarity, ignoring the outcome or treatment

response. As a consequence, the identified clusters may be phenotypically distinct but heterogeneous with respect to treatment effects, limiting their utility for prescriptive decision-making (Figure 1(a, left)).

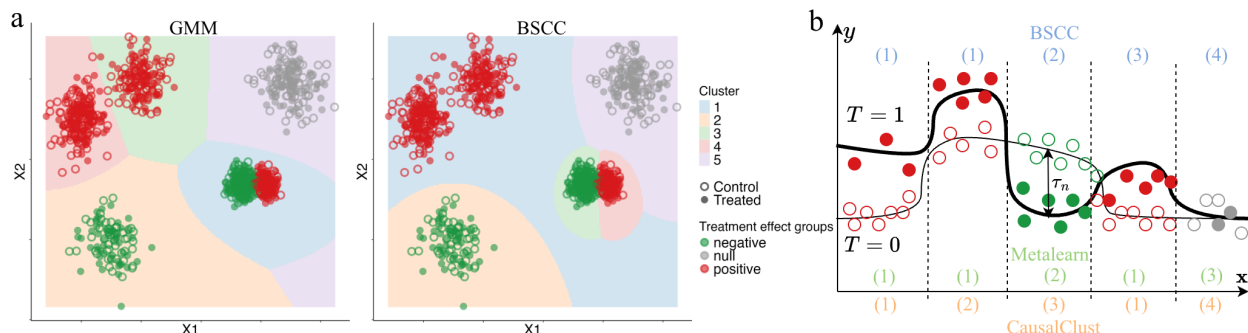


Figure 1: (a) Illustrating the conceptual difference between (left) unsupervised clustering with Gaussian Mixture Model (GMM) (right) supervised clustering with BSCC. GMM fails to recover the subgroups relevant to treatment while BSCC can. (b) Difference between BSCC clustering samples based on both covariates and treatment effect in a supervised clustering set-up, as opposed to causal clustering or supervised learning based approaches clustering based on potential outcomes or treatment effect only.

To address this limitation, recent methodological research has shifted toward supervised clustering, which incorporates outcome information into the clustering process to ensure that the discovered groups are predictive of the target variable [Rouanet et al., 2023]. However, most existing supervised clustering methods focus on predicting an outcome rather than on predicting the difference between two potential outcomes. In the context of precision medicine, it might also be beneficial to identify groups with different responses to an intervention (i.e., predictive enrichment) alongside those with different outcomes (i.e., prognostic enrichment) [Temple, 2010]. This motivates the development of *supervised causal clustering*, where subgroup discovery is guided jointly by covariate similarity and treatment-effect variation. Such a framework offers a promising path toward discovering subgroups that are both interpretable in terms of patient characteristics and actionable in terms of distinct treatment responses.

Related Work We summarize existing approaches for subgroup discovery in Table 1. *Unsupervised clustering* (UC) methods cluster patients based on covariate similarity alone, ignoring treatment response [Fraley and Raftery, 2002, Collins and Lanza, 2010]. While useful for exploratory analysis, they do not guarantee that the resulting clusters exhibit homogeneous treatment effects.

Supervised clustering with outcome (SC) as side information, including Bayesian profile regression [Molitor et al., 2010] and supervised GMM (SGMM) [Shou et al., 2019, Lyu et al., 2024], jointly model covariates for clustering while predicting outcomes via fixed effects. Extensions accommodate various outcome types, e.g., categorical and count data [Liverani et al., 2015] and longitudinal outcomes [Rouanet et al., 2023]. However, treatment effect has not been the primary focus of these studies, and they typically model the conditional expectation of the outcome rather than the contrast between potential outcomes.

Tree-based subgroup analysis (SA) methods, including interaction trees (IT) [Xiaogang et al., 2008] and model-based recursive partitioning (MOB) [Zeileis et al., 2008, Seibold et al., 2016], partition the covariate space recursively based on treatment effect heterogeneity. While directly supervised by treatment effect, these greedy and deterministic approaches may miss subgroups defined

Table 1: Summary of approaches. **TE**: treatment-effect-based.

Category	Supervised	Probabilistic	Covariate-based	TE	Example
UC	×	✓	✓	×	GMM
SC	✓	✓	✓	×	SGMM
SA	✓	×	✓	✓	IT, MOB
	✓	✓	✓	✓	BSCC (ours)
EM	✓	×	×	✓	CF, BART, DR-L, R-L, FINDIT, OWE, CC
BM	✓	✓	×	✓	Xu et al. [2016], Shahn and Madigan [2017]

by complex variable interactions or soft boundaries, and can be unstable [Thelen and Hennessy, 2025].

Effect modeling (EM) methods estimate individual treatment effects (ITE) using meta-learners [Kennedy, 2023]: doubly robust learner (**DR-LEARNER**) [Kennedy, 2020] and residual-learner (**R-LEARNER**) [Nie and Wager, 2020]; causal forests (**CF**) [Athey et al., 2019], Bayesian additive regression trees (**BART**) [Sparapani et al., 2021], or penalized regressions like Finding Heterogeneous Treatment Effects (**FINDIT**) [Imai and Ratkovic, 2013] and Outcome Weighted Estimation (**OWE**) [Chen et al., 2017]. While these methods provide flexible effect estimates at an individual level, they lack interpretable subgroup structures. Recovering subgroups from ITE estimates typically requires a post-hoc clustering step, [Bonvini et al., 2023]. *Causal clustering* (**CC**) [Kim et al., 2024] clusters individuals based on their potential outcomes estimated via counterfactual regression. This approach disentangles the potential outcome structure but ignores the covariate structure, potentially conflating structurally distinct subpopulations that happen to share similar potential outcomes (Figure 1(b)).

Bayesian methods (BM) have been used to capture HTE without focusing on finding subgroups in the covariate space. Xu et al. [2016] use mixture modelling to group longitudinal treatment effects, and Shahn and Madigan [2017] captures treatment heterogeneity as a mixture model.

Contributions We propose Bayesian Supervised Causal Clustering, or **BSCC** (“basic”), as a probabilistic framework for operationalizable patient stratification. BSCC jointly clusters individuals based on both their covariate structure and their response to treatment. Unlike traditional unsupervised clustering methods that only consider covariate similarity, or traditional effect modelling methods that focus on ITE estimation without finding subgroups, or causal clustering methods that do not consider covariate structure, BSCC explicitly integrates causal effect as a supervisory signal into the clustering process. Similar to tree-based subgroup analysis, this allows for the identification of subgroups that are homogeneous in covariates and treatment effects, but with more flexible subgroups through Bayesian mixture modelling. We explore the effectiveness of BSCC in both simulated and real datasets extensively, demonstrating that it can identify meaningful and consistent subgroups of individuals.

2 Methods

Standard mixture model with K components is described as

$$p(\mathbf{x}_n) = \sum_{k=1}^K p(z_n = k)p(\mathbf{x}_n | z_n = k) = \sum_{k=1}^K \pi_k p(\mathbf{x}_n | \boldsymbol{\theta}_k)$$

where $\mathbf{x}_n \in \mathbb{R}^D$ is the covariate vector for individual n , π_k is the probability of the k -th mixture component and $\boldsymbol{\theta}_k$ is the parameter of the respective component. z_n is the latent cluster assignment for the individual. When incorporating the information from outcome variable y , the supervised mixture model [Shou et al., 2019] is described as

$$p(y_n, \mathbf{x}_n) = \sum_{k=1}^K \pi_k p(\mathbf{x}_n | \boldsymbol{\theta}_k) p(y_n | \mathbf{x}_n, \boldsymbol{\beta}_k)$$

where $\boldsymbol{\beta}_k$ is a cluster-specific parameter capturing the relationship between covariates and outcome.

Consider we have observed data $\mathcal{D} = \{\mathbf{x}_n, y_n^{\text{obs}}, a_n\}_{n=1}^N$ where a denotes the binary treatment assignment. We denote the potential outcomes for treatment $a_n = 0$ and $a_n = 1$ as y_n^0 and y_n^1 respectively, where either y_n^0 or y_n^1 are observed in practice. Since we do not observe treatment effects $\tau_n^{\text{obs}} = y_n^1 - y_n^0$, we cannot directly use this as outcome in the supervised clustering framework. Instead, we model $p(y^{\text{obs}}, a, \mathbf{x})$, and parameterize each cluster based on their covariates and treatment effect, i.e.,

$$p(y_n^{\text{obs}}, a_n, \mathbf{x}_n) = \sum_{k=1}^K \pi_k p(\mathbf{x}_n | \boldsymbol{\theta}_k) p(a_n | \mathbf{x}_n, \boldsymbol{\zeta}) p(y_n^{\text{obs}} | a_n, \mathbf{x}_n, \boldsymbol{\phi}, \boldsymbol{\beta}_k)$$

where $p(a | \mathbf{x}, \boldsymbol{\zeta})$ denotes the propensity score, and we assume it to be independent of clusters.

For simplicity, we assume *randomization*, i.e., $p(a | \mathbf{x}) = p(a)$, meaning every individual has the same non-zero probability of receiving treatment [Sävje, 2021] implying

$$p(y_n^{\text{obs}}, a_n, \mathbf{x}_n) \propto \sum_{k=1}^K \pi_k p(\mathbf{x}_n | \boldsymbol{\theta}_k) p(y_n^{\text{obs}} | a_n, \mathbf{x}_n, \boldsymbol{\phi}, \boldsymbol{\beta}_k).$$

Randomization is a stricter condition that implies unconfoundedness, i.e., $(Y^0, Y^1) \perp\!\!\!\perp A | X$. While we focus on randomized settings, the framework naturally extends to observational data by modelling the propensity score explicitly [Li et al., 2023].

Potential Outcomes Assuming *Stable Unit Treatment Value Assumption (SUTVA)* (i.e., no interference and no hidden variation of treatment),

$$y_n^{\text{obs}} = y(a_n) = a_n y_n^1 + (1 - a_n) y_n^0,$$

and assuming the outcome to be continuous, we parameterize the potential outcomes as

$$\begin{aligned} y_n^0 &= \mu^0(\mathbf{x}_n; \boldsymbol{\phi}) + \epsilon_0 \\ y_n^1 &= \mu^0(\mathbf{x}_n; \boldsymbol{\phi}) + \tau(\mathbf{x}_n; \boldsymbol{\beta}_k) + \epsilon_1 \end{aligned}$$

with $\epsilon_0 \sim \mathcal{N}(0, \sigma_0^2)$, and $\epsilon_1 \sim \mathcal{N}(0, \sigma_1^2)$. Additionally, $(\epsilon_0, \epsilon_1) \perp\!\!\!\perp A$ due to randomization. Therefore,

$$y_n^{\text{obs}} | a_n, \mathbf{x}_n, \boldsymbol{\phi}, \boldsymbol{\beta}_k \sim \mathcal{N}(\mu^0(\mathbf{x}_n; \boldsymbol{\phi}) + a_n \tau(\mathbf{x}_n; \boldsymbol{\beta}_k), a_n \sigma_1^2 + (1 - a_n) \sigma_0^2).$$

Here $\tau(\cdot; \boldsymbol{\beta}_k)$ captures the treatment effects at each cluster k while the control outcome $\mu^0(\cdot; \boldsymbol{\phi})$ does not depend on the cluster.

Generative Process Thus, given K clusters, we consider the following generative framework (Figure 2),

$$\begin{aligned}
z_n &\sim \text{Cat}(\boldsymbol{\pi}) \\
\mathbf{x}_n &\sim f(\boldsymbol{\theta}_{z_n}) \\
\mu_n^0 &= \mu^0(\mathbf{x}_n; \boldsymbol{\phi}) \\
\tau_n &= \tau(\mathbf{x}_n; \boldsymbol{\beta}_{z_n}) \\
y_n^{\text{obs}} &\sim \mathcal{N}(\mu_n^0 + a_n \tau_n, a_n \sigma_1^2 + (1 - a_n) \sigma_0^2).
\end{aligned}$$

where $f(\boldsymbol{\theta}_k)$ represents a density function of mixed-type covariates, where we assume a normal distribution, i.e., $\mathcal{N}(\theta_{dk}^\mu, \theta_{dk}^\sigma)$ for d -th continuous variable, and a Bernoulli (or multinomial for categorical) distribution, i.e., $\text{Bern}(\theta_{dk}^p)$ for d -th binary variable. We do not explicitly model $p(a)$ due to randomization.

Adaptation to Binary Outcome The outcome can also be assumed to be binary, e.g., “death”, i.e., $y^{\text{obs}} \in \{0, 1\}$. In this context, we modify the output distributions as follows,

$$y_n^{\text{obs}} \sim \text{Bern}(\text{logit}^{-1}(\mu_n^0 + a_n \tau_n))$$

where the individual treatment effect is given as $\tau_n = \log p_n^1 / (1 - p_n^1) - \log p_n^0 / (1 - p_n^0) = \log \{p_n^1 / (1 - p_n^1)\} / \{p_n^0 / (1 - p_n^0)\}$, i.e., the log odds ratio (log OR) if we define the individual probability of death under control and treated groups to be p_n^0 and p_n^1 respectively.

Gaussian Process Prior on Control Outcome We use a Gaussian process (GP) to fit the nonlinear relationship $\mu^0(\mathbf{x}; \boldsymbol{\phi})$. A Gaussian process can be interpreted as providing a probability distribution over functions i.e. $\mu^0(\mathbf{x}) \sim \text{GP}(m_0(\mathbf{x}), \kappa_0(\mathbf{x}, \mathbf{x}'))$. For N noise-free potential outcomes $\{\mu_n^0\}_{n=1}^N$ paired with $\{\mathbf{x}_n\}_{n=1}^N$ input covariates, it is a multivariate Gaussian on these finite number of outcomes $\boldsymbol{\mu}^0 \in \mathbb{R}^N$ conditioned on their covariates: $\boldsymbol{\mu}^0 | \mathbf{X} \sim \mathcal{N}_N(\mathbf{m}_0, \mathbf{K}_0(\mathbf{X}))$ where $\mathbf{m}_0 = \mathbf{0}$ is an N -vector of unknown function values and $\mathbf{K}_0(\mathbf{X})$ is an $N \times N$ covariance matrix. We use the squared exponential kernel with noise for the covariance function, with the marginal standard deviation (α), controlling the overall scale of function values and length-scale (ρ), determining how far apart inputs must be before their function values become uncorrelated. To capture varying influence across covariates, we adopt separate length scales for each dimension, following the automatic relevance determination (ARD) approach [Neal, 1996]. Thus, GP parameters $\boldsymbol{\phi} = \{\alpha, \boldsymbol{\rho}\}$. Note that it is possible to use a linear kernel for GP to consider a simpler linear regression fit.

Choices for Treatment Effect For better interpretability, we consider a constant treatment effect over each cluster $\tau(\mathbf{x}; \boldsymbol{\beta}_k) = \tau_k = \beta_k$. This homogeneity assumption is analogous to conventional risk stratification approaches in clinical trials, where sample sizes are small and constant treatment effects are commonly assumed across risk strata [Kent et al., 2020]. We can also consider a linear treatment effect [Shahn and Madigan, 2017], i.e., $\tau(\mathbf{x}; \boldsymbol{\beta}_k) = \boldsymbol{\beta}_k^\top \mathbf{x}$, but focus on the former in this paper. Intuitively, we jointly cluster samples based on their covariates and their treatment effect as shown in Figure 1(b, right). The assumption of a normal distribution and a constant treatment effect facilitates interpretability and coherence by yielding clusters with spherical geometry and within each cluster, individuals share the same treatment-response characteristics.

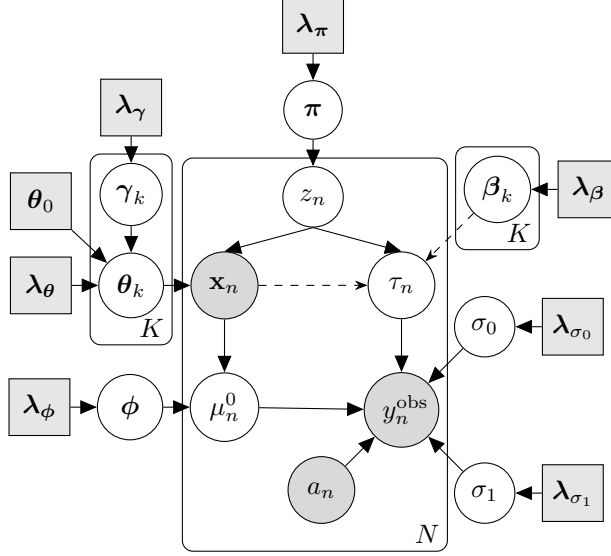


Figure 2: Plate Diagram of BSCC with feature selection.

Feature Selection Following the approach by [Liverani et al. \[2015\]](#), we employ the cluster-specific soft feature selection approach. Each mixture component k has an associated vector $\gamma_k = (\gamma_{k,1}, \dots, \gamma_{k,D})$, where $\gamma_{k,d}$ is a latent variable in $(0, 1)$ that determines whether the d -th covariate is important to mixture component k . For the binary covariates, let θ_{d0}^p be the sample prevalence of binary covariate d over the population, then we define the new composite cluster parameters as $\bar{\theta}_{dk}^p := \gamma_{k,d}\theta_{dk}^p + (1 - \gamma_{k,d})\theta_{d0}^p$. This expression is substituted in place of θ_{dk}^p to provide the likelihood for the covariate model. We further consider a weakly informative prior for $\gamma_{k,d} \sim \text{Beta}(0.5, 0.5)$. Similarly, for continuous covariates, we define θ_{d0}^μ to be sample mean of continuous covariate d , and define new cluster parameters as $\bar{\theta}_{dk}^\mu := \gamma_{k,d}\theta_{dk}^\mu + (1 - \gamma_{k,d})\theta_{d0}^\mu$.

Implementation We implement BSCC in RSTAN [[Stan Development Team, 2025](#)] using Automatic Differentiation Variational Inference (ADVI) [[Kucukelbir et al., 2017](#)]. We use non-informative priors for π and θ_k , half-normal priors with mean 0 and small standard deviation (0.01) for the noise standard deviations σ_0, σ_1 to regularize them toward small values, and $\beta_k \sim \mathcal{N}(0, 1)$ for the treatment effect by default (sensitivity analysis in Suppl. Tables [B.4](#) and [B.5](#)). The GP hyperparameters λ_ϕ ($\phi = \{\alpha, \rho\}$) are set by first fitting a GP to the control outcome data via maximum likelihood estimation [[Roustant et al., 2012](#)], and cluster-specific parameters θ_k are initialized using a Gaussian Mixture Model (GMM). Since Bayesian mixture models are known to suffer from posterior multimodality [[Mena and Walker, 2015](#), [Stephens, 1996](#), [Carreira-Perpiñán and Williams, 2003](#)], which can trap variational optimization in poor local optima, we run ADVI in parallel with diverse random initializations and select the solution with the highest evidence lower bound (ELBO).

3 Simulation Results

Metrics We calculate the Adjusted Rand Index (ARI) to assess the clustering performance in the covariate space. Since different methods produce results in different forms, we report the range of Subgroup-specific Average Treatment Effects (SATEs) on the test data as a common metric to evaluate how well each method separates subgroups with distinct treatment effects. SATE is computed

after assigning individuals to their respective clusters, and we expect that supervised causal clustering with treatment effect as supervision (e.g., BSCC) should find clusters with more distinct treatment effects. Additionally, to assess the performance of ITE estimation, we compute the Precision in Estimation of Heterogeneous Effects (PEHE) [Hill, 2011]: $PEHE = \sqrt{\frac{1}{N} \sum_{i=n}^N (\tau_n - \mathbb{E}[y_n^1 - y_n^0 | \mathbf{x}_n])^2}$.

Null Treatment Effects (SIMULATION NULL) We evaluate BSCC under a setting where all individuals share a single cluster with zero treatment effect. Since BSCC clusters jointly over covariates and treatment outcomes, it may still identify covariate-driven clusters when no treatment heterogeneity exists. As shown in Suppl. Table B.6, when $K > 1$, the model finds clusters with divergent estimated treatment effects τ_k on training data (e.g., range $[-0.69, 1.23]$ for $K = 4$), but the corresponding test SATE ranges remain close to zero (e.g., $[-0.14, 0.03]$), indicating that the apparent heterogeneity does not generalise. Moreover, $K = 1$ yields the lowest test PEHE, confirming the absence of heterogeneity. This highlights the importance of model selection: choosing the correct K via validation avoids false positive discovery of spurious treatment effect heterogeneity.

Feature Selection (SIMULATION FS) To illustrate this, we simulated a two-dimensional dataset with four clusters but two different constant treatment effect groups as shown in Suppl. Figure B.1a. In this case, only the first dimension or feature plays a significant role in clustering when considering treatment effects as the outcome, since the cluster means of the second feature are both close to the sample mean. The learned feature importance with BSCC for each cluster is shown in Suppl. Figure B.1b, where we see relatively larger weight for the first feature (> 0.5) and small weight for the second feature (< 0.1) with an ARI of 0.88.

Subgroup Discovery with HTE (SIMULATION HTE) We simulate a toy dataset consisting of $N = 1200$ samples with 12 covariates, including 6 binary variables, to show the difference among various methods. Control outcomes are generated using a nonlinear function (detailed in Suppl. B.2), and the treated group comprises 50% of the population. We manually construct 5 clusters with specific properties, as visualized in Figure 3(a): (1) Clusters 2 ($\tau_2 = 5$, orange) and 3 ($\tau_3 = -5$, green) are close in covariate space but have opposite treatment effects; (2) Clusters 4 ($\tau_4 = 0$, red) and 5 ($\tau_5 = 0$, purple) are well-separated yet share the same null treatment effect; and (3) Cluster 1 ($\tau_1 = 0.5$, blue) is distinct from the others but exhibits a near-null treatment effect similar to Clusters 4 and 5. Our goal is to recover 4 clusters with distinct treatment effects, as Clusters 4 and 5 share a null effect. Additionally, we generate a parallel dataset with identical settings but a smaller proportion of treated units (20%) to evaluate sensitivity to treatment assignment imbalance. We split the data equally into training and test sets.

Table 2 summarises the results from SIMULATION HTE, evaluating the performance of BSCC, along with comparisons to (1) GMM and (2) SGMM with treated outcome as supervision only. Moreover, we also benchmark BSCC against widely used supervised learning approaches: (3) IT, (4) MOB, (5) CF, (6) BART, (7) DR-LEARNER, (8) R-LEARNER, (9) FINDIT, (10) OWE, and (11) CC, evaluated on balanced simulated datasets with treatment proportion 0.5. Cluster labels for effect modeling and causal clustering methods are obtained by applying GMM to estimated treatment effects or potential outcomes, respectively. For each method, we identify four clusters. ITEs for clustering-based methods are approximated by SATEs.

We find that BSCC attains a moderate ARI of 0.721, compared to 0.768 for GMM. However, GMM produces SATE estimates that fail to reflect the true heterogeneity (range $[-0.40, 1.32]$ versus the ground truth $[-5, 5]$), highlighting a fundamental tension between clustering fidelity in covariate space and treatment effect estimation. In terms of SATE, BSCC produces estimates that closely

Table 2: Summary of performance for SIMULATION HTE.

Model (Treat Prop.)	ARI	SATE	PEHE
GMM (0.5)	0.768	[-0.40, 1.32]	3.13
SGMM (0.5)	0.625	[-5.54, 0.67]	2.65
IT (0.5)	0.574	[-0.03, -0.03]	3.09
MOB (0.5)	0.437	[-4.73, 2.38]	2.58
BSCC (0.2)	0.715	[-4.99, 3.98]	1.49
BSCC (0.5)	0.721	[-5.13, 3.99]	1.45
CF (0.5)	0.544	[-4.71, 3.67]	1.98
BART (0.5)	0.381	[-4.46, 4.61]	1.86
DR-LEARNER (0.5)	0.548	[-4.56, 4.25]	2.14
R-LEARNER (0.5)	0.508	[-4.78, 3.57]	1.72
FINDIT (0.5)	0.126	[-0.33, 0.31]	3.95
OWE (0.5)	0.333	[-3.91, 2.22]	2.46
CC (0.5)	0.524	[-3.72, 3.76]	1.86

match the ground truth (range [-5.13, 3.99]), demonstrating superior fidelity in capturing subgroup-level heterogeneity. Among all methods, BSCC achieves the lowest test PEHE (1.45), outperforming the next-best R-LEARNER (1.72), BART and CC (1.86), and CF (1.98). Notably, methods such as IT and FINDIT yield near-degenerate SATE ranges, indicating a failure to capture heterogeneity in the test data. Performance for BSCC remains robust when the treated proportion is reduced to 0.2, with only a marginal increase in PEHE (1.49) and a slight decline in ARI (0.715).

To explore the difference among the various methods, as illustrated in Figure 3(b), GMM does not distinguish between Clusters 2 ($\tau_2 = 5$) and 3 ($\tau_3 = -5$), which are close in covariate space but have opposite treatment effects. In contrast, BSCC in Figure 3(e) separates them, while merging Clusters 4 and 5 that share the same null treatment effect.

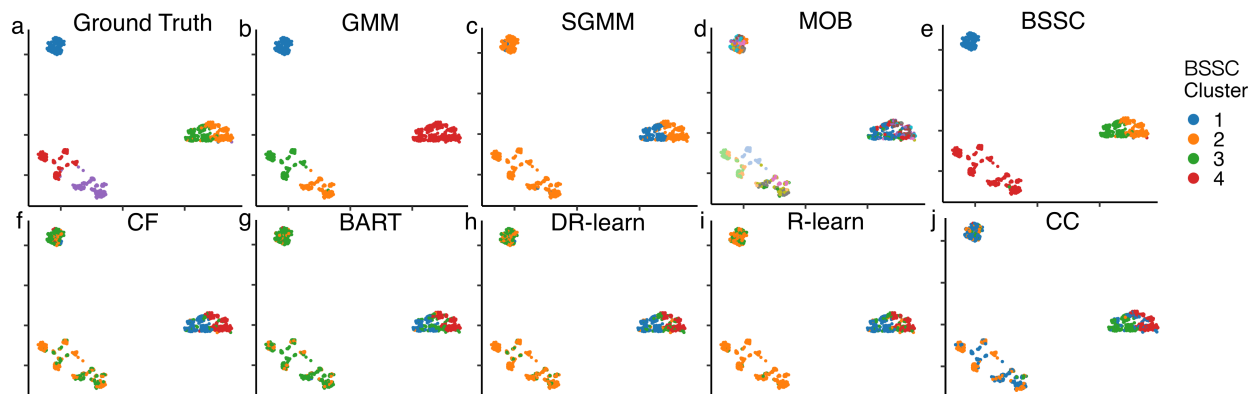


Figure 3: Visualization of UMAP Projection of the Simulated Dataset in SIMULATION HTE: Cluster assignments are given by (a) ground truth of constant treatment effects (0.5, 5, -5, 0, 0), (b) GMM, (c) SGMM, (d) MOB, (e) BSCC, (f) CF, (g) BART, (h) DR-LEARNER, (i) R-LEARNER and (j) CC.

In Figure 3(c), SGMM supervises clustering using only the treated outcome $\mathbb{E}[y^1] = \mathbb{E}[y^0] + \tau$ with noise. This limitation is best understood via Suppl. Figure B.2: projecting onto the y^1 axis (vertical), Cluster 3 (green, $\tau_3 = -5$) occupies a distinctly low range ($y^1 \approx -6$ to 1), making it easily separable. However, the remaining clusters overlap substantially along y^1 : Cluster 2 (orange, $\tau_2 = 5$) has $y^1 \approx 4$ –12, but because Clusters 2 and 3 share similar covariate distributions (and hence similar y^0), Cluster 2’s high treated outcome $y^0 + 5$ overlaps with Cluster 4 (red, $\tau_4 = 0$), whose higher baseline y^0 yields $y^1 \approx 3$ –9. Similarly, Clusters 1 and 5 overlap in y^1 . Without access to y^0 , SGMM cannot disentangle baseline response from treatment effect, and thus merges Clusters 1, 2, 4, and 5. This is reflected in its SATE range $[-5.54, 0.67]$, recovering only the negative effect.

For effect modeling methods (Figure 3(f,g,h,i)), many individuals are misclassified when clustering is based solely on estimated treatment effects. Subgroup analysis methods such as MOB (Figure 3(d)) tend to over-partition the data, producing more clusters than the ground truth due to their one-variable-at-a-time splitting strategy, and fail to capture interactions across multiple covariates. Causal clustering (Figure 3(j)) clusters on imputed potential outcome vectors (y^0, y^1); while it captures some structure, it cannot distinguish clusters that share similar potential outcomes but differ in covariate space (e.g., Clusters 1, 4 and 5), as further illustrated in Suppl. Figure B.2.

Prior Sensitivity of β_k We use the same simulated dataset as SIMULATION HTE. As shown in Table B.4, the model is robust to the choice of prior standard deviation: varying the SD from 0.5 to 100 yields stable ARI (0.73–0.75) and PEHE (0.85–0.99). Providing informative prior means closer to the true effects can slightly improve performance (Table B.5), though the default non-informative prior performs well.

4 Real Application

We assess the effectiveness of BSCC on the Third International Stroke Trial (IST-3), evaluating the benefit of thrombolysis in patients with acute ischaemic stroke [Sandercock et al., 2012]. Patients were either allocated to 0.9 mg/kg intravenous recombinant tissue plasminogen activator (rt-PA) or to control by placebo. The primary outcome used is the Oxford Handicap Score (OHS) at 6 months, which indicates if the patient is alive and independent, ranging from 0 to 6 with 6 representing death. We selected 12 features as covariates for clustering involving 6 continuous variables, based on findings from Sandercock et al. [2012], as detailed in Suppl. Table C.7. After dropping missing values in features, we have a total of 2737 patients. The proportion of observed OHS for control and treated groups is shown in Suppl. Figure C.4. We standardised continuous covariates and performed one-hot encoding for categorical covariates having categories greater than 2.

We split the dataset evenly into training and testing sets to ensure comparable sample sizes. To improve the modelling of control outcomes in the training set, we converted the outcome to a binary variable indicating “death”, corresponding to OHS= 6 in Figure C.4, which has the proportion of around 26%. We assume a constant treatment effect within each cluster, allowing it to be interpreted as log odds ratio (log OR) for binary outcomes. Model performance is evaluated using two metrics on the test data: the accuracy of predicted control outcomes and the policy risk [Shalit et al., 2017], which measures the expected outcome under a treatment policy $\text{POL}(\mathbf{x})$ that assigns each individual to the treatment arm with the better estimated effect. A lower policy risk indicates that the estimated treatment effects lead to better treatment decisions on held-out data: $R_{\text{POL}} = 1 - (\mathbb{E}[y^1 | \text{POL}(\mathbf{x}) = 1, a = 1]p(\text{POL}(\mathbf{x}) = 1) + \mathbb{E}[y^0 | \text{POL}(\mathbf{x}) = 0, a = 0]p(\text{POL}(\mathbf{x}) = 0))$.

We identified three clusters that exhibit relatively high accuracy in predicting control outcomes and low policy risk, as reported in Suppl. Table C.8. Since cluster assignments during testing are based solely on covariate information, it is important to assess the consistency between training and

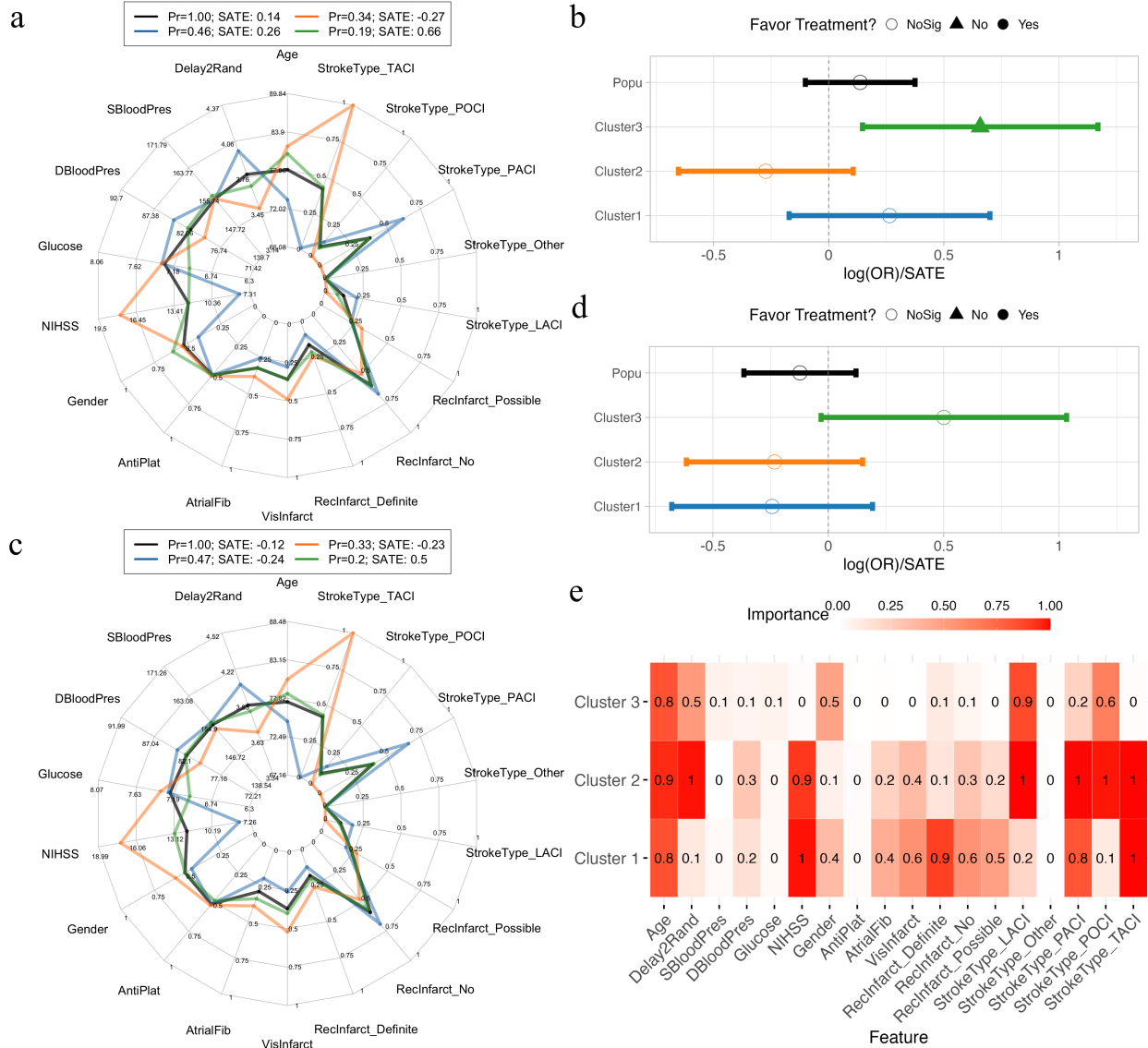


Figure 4: BSCC on IST-3 Dataset: (a) The estimated cluster means and (b) corresponding ORs with 95% CIs for training (in log scale), and (c) the empirical cluster means and (d) corresponding ORs with 95% CIs for test set. Each axis representing a continuous covariate in the radar chart is transformed back to its original scale to enhance interpretability. (e) Cluster-specific feature importance.

test results. Notably, when $K = 3$, the model yields consistent cluster means and odds ratios (ORs) across both sets, as illustrated in Figure 4.

We visualise the estimated cluster means given by the training dataset compared with the empirical cluster means obtained by cluster assignments for the test dataset in Figure 4(a) and (c). This helps with examining the differences and stability between learning and deploying this model. In addition, we also calculate the empirical ORs (SATE) with 95% confidence intervals (CIs) for each cluster to evaluate the tendency of each cluster towards the treatment in Figure 4(b) and (d).

The three identified clusters exhibit distinct prognostic profiles: **Cluster 1** comprises patients

with characteristics associated with a more favorable prognosis: younger age, lower NIH Stroke Scale (NIHSS) scores, a higher proportion with no visible ischaemia on CT scans, and predominantly milder stroke syndromes (partial anterior circulation and lacunar). This group has the lowest control arm mortality at 13.3%. Compared with the whole trial population, **Cluster 2** represents individuals with more severe strokes and additional poor prognostic indicators. These patients are older, have higher NIHSS scores, and almost exclusively exhibit total anterior circulation infarcts, the most severe stroke subtype. This cluster demonstrates the highest control arm mortality at 47.6%. **Cluster 3** largely reflects the overall trial population, but with a few distinctions: patients are moderately older, have lower blood glucose levels, and a higher proportion show definite ischaemia on CT scans, suggesting delayed presentation or diagnosis. The control arm mortality in this group is 22.8%, slightly lower than the overall trial population control group (25.9%).

Regarding feature importance, age and absence of lacunar stroke syndrome are most influential in Cluster 3. For Cluster 2, key features include age, delay to randomisation, NIHSS score, and stroke syndrome type. In Cluster 1, the most important variables are age, NIHSS, evidence of infarction on CT, and stroke subtype. These findings align with subgroup effects reported in the original trial by [Sandercock et al. \[2012\]](#), where HTE were identified for age, NIHSS, and predicted probability of poor 6-month outcome (driven by age and NIHSS). The pronounced HTE in Cluster 3 may reflect its higher prevalence of older individuals and elevated NIHSS scores.

Suppl. Figure C.5 shows the clustering results by the unsupervised clustering approach using GMM for comparison. We observe that when specifying $K = 3$, the GMM finds three clusters with log ORs very close to 0 i.e. range of SATE $[-0.01, 0.14]$. Although BSCC provides improvement in terms of identifying different treatment effect tendencies i.e. range of SATE $[-0.27, 0.66]$, the improvement is not statistically significant in the test dataset. Nevertheless, as shown in the figures in Suppl. C, supervised learning models often produce unstable subgroup structures, with log-odds ratio (SATE) estimates that vary considerably between training and test sets. The subgroup analysis method MOB identified four clusters using only the splitting covariates "NIHSS" and "age", while failing to account for clinically important covariates such as stroke subtypes, which were captured by BSCC.

5 Discussion

We presented a Bayesian supervised causal clustering framework (BSCC) that simultaneously models covariates and treatment responses. We apply BSCC in the RCT population to find meaningful subgroups aligned to heterogeneous treatment effects. This has several advantages over existing methods. While traditional subgroup analyses identify subgroups based on splitting covariate space or regressing with outcome labels, they do not directly find subgroups based on covariate similarities, resulting in clusters that do not capture interactions between covariates or overlapping clusters. Traditional clustering approaches, on the other hand, are capable of identifying similar covariate subgroups but may not align with treatment response heterogeneity. Causal clustering approaches directly cluster based on causal effects; however, the clustering structure might be less operationalizable. The supervised clustering methods utilize non-causal outcomes without considering causal structures. In contrast, BSCC explicitly incorporates treatment effects as outcome information, enabling principled identification of interpretable, operationalizable, and consistent subpopulations under treatment effect heterogeneity.

Empirical evaluations on synthetic datasets demonstrate the framework’s flexibility in handling mixed-type covariates with feature selections and nonlinear outcome models, as well as avoiding spurious discovery (discussed in SIMULATION NULL). Importantly, the model recovers meaningful

cluster structures even when traditional clustering and supervised clustering methods fail. For example, it distinguishes covariate-similar subgroups with opposing treatment effects and merges covariate-distant groups with shared treatment responses, capabilities that standard GMM and SGMM baselines lack. In real-world clinical data from the IST-3 stroke trial, our BSCC model uncovered three clinically meaningful clusters differentiated by age, stroke severity, and imaging biomarkers. These subgroups showed distinct mortality patterns and treatment responses, aligning with known clinical findings and supporting the model’s utility in health applications.

BSCC can be extended in various manners. Our current approach assumes randomized treatment assignment, and the approach can be extended to observational data settings. The current formulation considers a fully supervised set-up, and it can be extended BSCC to a semi-supervised clustering variation by disregarding the outcome information of unlabelled samples during training. We consider binary treatments with continuous or discrete outcomes, and the approach can be extended to consider multiple treatment arms and other outcome modalities, e.g., time-varying, time-to-event, etc. Finally, the method is currently implemented in ADVI, and can be extended to handle larger datasets with more tailored inference methods.

References

- Carla Abdelnour, Federica Agosta, Marco Bozzali, Bertrand Fougère, Atsushi Iwata, Ramin Nilforooshan, Leonel T. Takada, Félix Viñuela, and Martin Traber. Perspectives and challenges in patient stratification in Alzheimer’s disease. *Alzheimer’s Research & Therapy*, 14(1):112, August 2022. ISSN 1758-9193. doi: 10.1186/s13195-022-01055-y.
- Susan Athey, Julie Tibshirani, and Stefan Wager. Generalized random forests. *Annals of Statistics*, 47:1179–1203, 04 2019. doi: 10.1214/18-AOS1709.
- Matteo Bonvini, Zhenghao Zeng, Miaoqing Yu, Edward H. Kennedy, and Luke Keele. Flexibly Estimating and Interpreting Heterogeneous Treatment Effects of Laparoscopic Surgery for Cholecystitis Patients, 2023.
- Miguel Á. Carreira-Perpiñán and Christopher K. I. Williams. On the Number of Modes of a Gaussian Mixture. In *Scale Space Methods in Computer Vision*, pages 625–640. Springer Berlin Heidelberg, 2003. ISBN 978-3-540-44935-5.
- Shuai Chen, Lu Tian, Tianxi Cai, and Menggang Yu. A general statistical framework for subgroup identification and comparative treatment scoring. *Biometrics*, 73(4):1199–1209, December 2017. doi: 10.1111/biom.12676.
- Linda Collins and Stephanie Lanza. *Latent Class and Latent Transition Analysis: With Applications in the Social, Behavioral, and Health Sciences*. John Wiley and Sons, Inc., 01 2010. ISBN 978-0-470-22839-5. doi: 10.1002/9780470567333.indsub.
- Bruno Dubois, Alessandro Padovani, Ph Scheltens, Andrea Rossi, and Grazia Dell’Agnello. Timely Diagnosis for Alzheimer’s Disease: A Literature Review on Benefits and Challenges. *Journal of Alzheimer’s Disease*, 49:617–631, 10 2015. doi: 10.3233/JAD-150692.
- Chris Fraley and Adrian E Raftery. Model-Based Clustering, Discriminant Analysis, and Density Estimation. *Journal of the American Statistical Association*, 97(458):611–631, 2002. doi: <https://doi.org/10.1198/016214502760047131>.

- Qi Guo, Xiaoni Lu, Ya Gao, Jingjing Zhang, Bin Yan, Dan Su, Anqi Song, Xi Zhao, and Gang Wang. Cluster analysis: a new approach for identification of underlying risk factors for coronary artery disease in essential hypertensive patients. *Scientific Reports*, 7(1), Mar 2017. doi: <https://doi.org/10.1038/srep43965>.
- Jennifer L. Hill. Bayesian Nonparametric Modeling for Causal Inference. *Journal of Computational and Graphical Statistics*, 20(1):217–240, 2011. doi: 10.1198/jcgs.2010.08162.
- Kosuke Imai and Marc Ratkovic. Estimating treatment effect heterogeneity in randomized program evaluation. *The Annals of Applied Statistics*, 7, 05 2013. doi: 10.1214/12-AOAS593.
- Edward Kennedy. Optimal doubly robust estimation of heterogeneous causal effects, 04 2020.
- Edward Kennedy. Towards optimal doubly robust estimation of heterogeneous causal effects. *Electronic Journal of Statistics*, 17, 01 2023. doi: 10.1214/23-EJS2157.
- David M Kent, Ewout Steyerberg, and David van Klaveren. Personalized evidence based medicine: predictive approaches to heterogeneous treatment effects. *BMJ*, 363, 2018. ISSN 0959-8138. doi: 10.1136/bmj.k4245.
- David M Kent, Jessica K Paulus, David van Klaveren, Ralph D’Agostino, Steve Goodman, Rodney Hayward, John P A Ioannidis, Bray Patrick-Lake, Sally Morton, Michael Pencina, Gowri Raman, Joseph S Ross, Harry P Selker, Ravi Varadhan, Andrew Vickers, John B Wong, and Ewout W Steyerberg. The Predictive Approaches to Treatment effect Heterogeneity (PATH) Statement. *Annals of Internal Medicine*, 172(1):35–45, 2020. doi: 10.7326/M18-3667.
- Kwangho Kim, Jisu Kim, Larry A. Wasserman, and Edward H. Kennedy. Hierarchical and Density-based Causal Clustering. In A. Globerson, L. Mackey, D. Belgrave, A. Fan, U. Paquet, J. Tomczak, and C. Zhang, editors, *Advances in Neural Information Processing Systems*, volume 37, pages 30363–30393. Curran Associates, Inc., 2024.
- Richard Kravitz, Naihua Duan, and Joel Braslow. Evidence-Based Medicine, Heterogeneity of Treatment Effects, and the Trouble with Averages. *The Milbank quarterly*, 82:661–87, 02 2004. doi: 10.1111/j.0887-378X.2004.00327.x.
- Alp Kucukelbir, Dustin Tran, Rajesh Ranganath, Andrew Gelman, and David M. Blei. Automatic differentiation variational inference. *J. Mach. Learn. Res.*, 18(1):430–474, January 2017. ISSN 1532-4435.
- Fan Li, Peng Ding, and Fabrizia Mealli. Bayesian causal inference: a critical review. *Philosophical Transactions of the Royal Society A*, 381(2247):20220153, 2023. doi: 10.1098/rsta.2022.0153.
- Silvia Liverani, David I. Hastie, Lamiae Azizi, Michail Papathomas, and Sylvia Richardson. PR-MiuM: An R Package for Profile Regression Mixture Models Using Dirichlet Processes. *Journal of Statistical Software*, 64(7):1–30, 2015. doi: 10.18637/jss.v064.i07.
- Ziyang Lyu, Daniel Ahfock, Ryan Thompson, and Geoffrey J. McLachlan. Semi-supervised Gaussian mixture modelling with a missing-data mechanism in R, 2024.
- Ramsés H. Mena and Stephen G. Walker. On the Bayesian Mixture Model and Identifiability. *Journal of Computational and Graphical Statistics*, 24(4):1155–1169, 2015. ISSN 10618600.

- John Molitor, Michail Papathomas, Michael Jerrett, and Sylvia Richardson. Bayesian profile regression with an application to the National survey of children’s health. *Biostatistics*, 11(3):484–498, 07 2010. ISSN 1465-4644. doi: 10.1093/biostatistics/kxq013.
- Kevin P. Murphy. *Machine Learning: A Probabilistic Perspective*. The MIT Press, 2012. ISBN 0262018020.
- Radford M. Neal. *Bayesian learning for neural networks*. Lecture notes in statistics ; 118. Springer, New York, 1996. ISBN 0387947248.
- X Nie and S Wager. Quasi-oracle estimation of heterogeneous treatment effects. *Biometrika*, 108(2):299–319, 09 2020. ISSN 0006-3444. doi: 10.1093/biomet/aaa076.
- Anais Rouanet, Rob Johnson, Magdalena Strauss, Sylvia Richardson, Brian D Tom, Simon R White, and Paul D W Kirk. Bayesian profile regression for clustering analysis involving a longitudinal response and explanatory variables. *Journal of the Royal Statistical Society Series C: Applied Statistics*, 73(2):314–339, 11 2023. ISSN 0035-9254. doi: 10.1093/jrsssc/qlad097.
- Olivier Roustant, David Ginsbourger, and Yves Deville. DiceKriging, DiceOptim: Two R packages for the analysis of computer experiments by kriging-based metamodeling and optimization. *Journal of Statistical Software*, 51(1):1–55, 2012.
- P Sandercock, JM Wardlaw, RI Lindley, M Dennis, G Cohen, G Murray, K Innes, G Venables, A Czlonkowska, A Kobayashi, S Ricci, V Murray, E Berge, KB Slot, Hankeymm GJ, M Correia, A Peeters, K Matz, P Lyrer, G Gubitz, SJ Phillips, A Arauz, IST-3 collaborative group, R Al-Shahi Salman, and S Lewis. The benefits and harms of intravenous thrombolysis with recombinant tissue plasminogen activator within 6 h of acute ischaemic stroke (the third international stroke trial [IST-3]): a randomised controlled trial. *The Lancet*, 379(9834):2352–2363, 2012. ISSN 0140-6736. doi: [https://doi.org/10.1016/S0140-6736\(12\)60768-5](https://doi.org/10.1016/S0140-6736(12)60768-5).
- Heidi Seibold, Achim Zeileis, and Torsten Hothorn. Model-Based Recursive Partitioning for Subgroup Analyses. *The International Journal of Biostatistics*, 12, 05 2016. doi: 10.1515/ijb-2015-0032.
- Christopher W. Seymour, Jason N. Kennedy, Shu Wang, Chung-Chou H. Chang, Corrine F. Elliott, Zhongying Xu, Scott Berry, Gilles Clermont, Gregory Cooper, Hernando Gomez, David T. Huang, John A. Kellum, Qi Mi, Steven M. Opal, Victor Talisa, Tom van der Poll, Shyam Visweswaran, Yoram Vodovotz, Jeremy C. Weiss, Donald M. Yealy, Sachin Yende, and Derek C. Angus. Derivation, Validation, and Potential Treatment Implications of Novel Clinical Phenotypes for Sepsis. *JAMA*, 321(20):2003–2017, 05 2019. ISSN 0098-7484. doi: 10.1001/jama.2019.5791.
- Zach Shahn and David Madigan. Latent class mixture models of treatment effect heterogeneity. *Bayesian Analysis*, 12(3):831–854, 2017. doi: 10.1214/16-BA1022.
- Uri Shalit, Fredrik D. Johansson, and David Sontag. Estimating individual treatment effect: generalization bounds and algorithms. In Doina Precup and Yee Whye Teh, editors, *Proceedings of the 34th International Conference on Machine Learning*, volume 70 of *Proceedings of Machine Learning Research*, pages 3076–3085. PMLR, 06–11 Aug 2017.
- Yahya Shehabi, Ary Serpa Neto, Belinda Howe, Rinaldo Bellomo, Yaseen Arabi, Michael Bailey, Frances Bass, Suhaini Kadiman, Colin McArthur, Michael Reade, Ian Seppelt, Jukka Takala, Matt Wise, and Steve Webb. Early sedation with dexmedetomidine in ventilated critically ill patients

- and heterogeneity of treatment effect in the SPICE III randomised controlled trial. *Intensive Care Medicine*, 47, 03 2021. doi: 10.1007/s00134-021-06356-8.
- Xiao Shou, Georgios Mavroudeas, Alexander New, Kofi Arhin, Jason N. Kuruzovich, Malik Magdon-Ismail, and Kristin P. Bennett. Supervised Mixture Models for Population Health. In *2019 IEEE International Conference on Bioinformatics and Biomedicine (BIBM)*, pages 1057–1064, 2019. doi: 10.1109/BIBM47256.2019.8983339.
- Pratik Sinha, Kevin L. Delucchi, B. Taylor Thompson, Daniel F. McAuley, Michael A. Matthay, Carolyn S. Calfee, and for the NHLBI ARDS Network. Latent class analysis of ARDS subphenotypes: a secondary analysis of the statins for acutely injured lungs from sepsis (SAILS) study. *Intensive Care Medicine*, 44(11):1859–1869, November 2018. ISSN 1432-1238. doi: 10.1007/s00134-018-5378-3.
- Rodney Sparapani, Charles Spanbauer, and Robert McCulloch. Nonparametric Machine Learning and Efficient Computation with Bayesian Additive Regression Trees: The BART R Package. *Journal of Statistical Software*, 97(1):1–66, 2021. doi: 10.18637/jss.v097.i01.
- Stan Development Team. RStan: the R interface to Stan, 2025. URL <https://mc-stan.org/>. R package version 2.26.24.
- Matthew Stephens. Dealing with the Multimodal Distributions of Mixture Model Parameters. *Preprint, Department of Statistics, University of Oxford*, 1996.
- Fredrik Sävje. Randomization does not imply unconfoundedness, 2021.
- R Temple. Enrichment of Clinical Study Populations. *Clinical Pharmacology & Therapeutics*, 88(6):774–778, 2010. doi: <https://doi.org/10.1038/clpt.2010.233>.
- Haedi Thelen and Sean Hennessy. Characterizing Treatment Effect Heterogeneity Using Real-World Data. *Clinical Pharmacology & Therapeutics*, 117(5):1209–1216, 2025. doi: <https://doi.org/10.1002/cpt.3627>.
- Su Xiaogang, Zhou Tianni, Yan Xin, Fan Juanjuan, and Yang Song. Interaction Trees with Censored Survival Data. *The International Journal of Biostatistics*, 4(1):1–28, January 2008. doi: 10.2202/1557-4679.1071.
- Yanbo Xu, Yanxun Xu, and Suchi Saria. A Bayesian nonparametric approach for estimating individualized treatment-response curves. In *Proceedings of the 1st Machine Learning for Healthcare Conference*, volume 56 of *Proceedings of Machine Learning Research*, pages 282–300. PMLR, 2016.
- Achim Zeileis, Torsten Hothorn, and Kurt Hornik. Model-Based Recursive Partitioning. *Journal of Computational and Graphical Statistics*, 17(2):492–514, 2008. doi: 10.1198/106186008X319331.

Bayesian Supervised Causal Clustering (Supplementary Material)

A Additional Model Information

Table A.1: Summary of Related Works

Group based on	Task	Example	Covariate Split	Supervision
Clustering covariates	Unsupervised	GMM, LCA	Multivariate	None
	Supervised	BayesProfile, SGMM	Multivariate	Outcome
	Supervised	IT, MOB	One-at-a-time	Treatment effect
	Supervised	BSCC	Multivariate	Treatment effect
Clustering treatment effects	Supervised	Meta-learners, CF, BART, FINDIT, OWE	None	Treatment effect
Clustering potential outcomes	Supervised	Causal Clustering	None	Potential outcomes

In our model, we assume: (1) multiple covariates are independent and continuous covariates are distributed by Gaussian while binary covariates are distributed by Bernoulli. (2) one binary treatment variable i.e. control or treated; (3) scalar continuous outcome variables for control and treated groups for supervision, although it is easy for our model to extend to binary outcome variables by applying a sigmoid function (binary outcome variable is used for the real dataset). For example in tabular data, it might be Table A.2.

Table A.2: Example Tabular Data for HTE

ID	Gender	Age	Treated	Control Outcome	Treated Outcome
1	F	61	Yes	NA	2
2	M	35	No	1	NA
3	F	46	Yes	NA	1

B Additional Simulation Results

B.1 Sanity Check

We simulate our test datasets for the simplest linear (L) or constant (C) cases of control outcome functions and treatment effects for a sanity check. The number of covariates used is 9, including 3 binary variables. The ground truth number of clusters for all four datasets is 5. We calculate the Adjusted Rand Index (ARI) to assess the clustering accuracy as shown in Table B.3. The average relative L_2 error is computed by taking means of relative L_2 errors for $\{\{\boldsymbol{\theta}_k, \boldsymbol{\beta}_k\}_{k=1}^K, \boldsymbol{\pi}, \boldsymbol{\mu}^0\}$, reflecting the estimation accuracy of parameters.

Table B.3: A Summary of Synthetic Datasets and Model Performance for Sanity Check of BSCC: The data case of L-C (i.e. linear-constant) means the data is generated from a linear control outcome function and constant treatment effects for each cluster.

Size	Data Case (Treated Prop.)	Avg. Rel. L_2 Error	ARI
$N = 720$	L-C (0.5)	0.04	1
$N = 740$	L-C (0.2)	0.033	0.996
$N = 760$	L-L (0.5)	0.072	1
$N = 780$	L-L (0.2)	0.054	0.996

Our model demonstrates strong performance across all four datasets, with small average relative L_2 error (< 0.08) and ARIs all close to 1, which assumes a linear control outcome function, particularly when a linear kernel is used for the Gaussian process prior. Additionally, when adopting an exponentiated quadratic (RBF) kernel with carefully tuned hyperparameters, the model achieves near-perfect clustering and treatment effect estimation accuracy. For the demonstration of feature selection technique, Figure B.1b shows the learned cluster-specific feature importance.

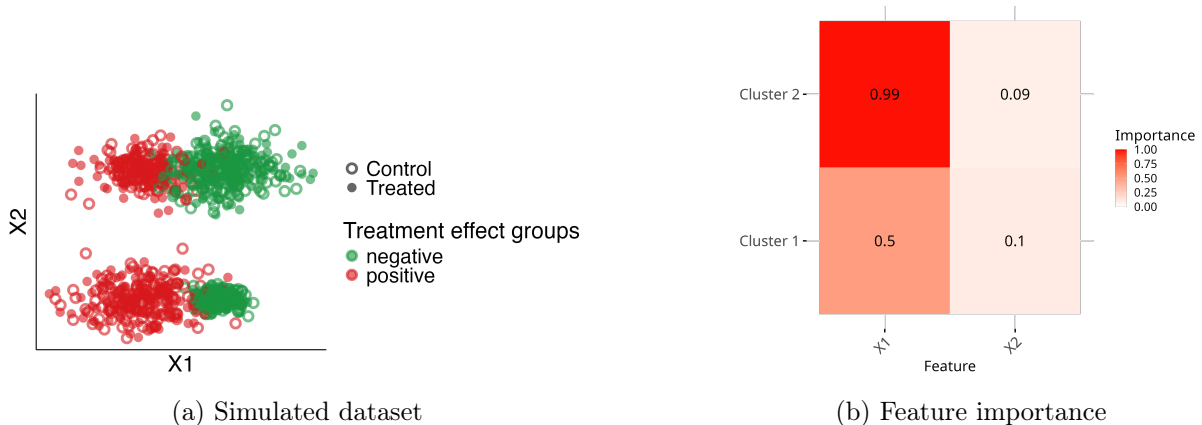


Figure B.1: SIMULATION FS: (a) Simulated dataset and (b) learned cluster-specific feature importance by BSCC.

B.2 HTE Comparison to Supervised Learning Methods

The SIMULATION HTE dataset consists of $N = 1200$ individuals with $D = 12$ covariates (6 continuous, 6 binary), drawn from 5 clusters with mixing proportions $\pi \approx (0.19, 0.21, 0.17, 0.21, 0.22)$. Continuous covariates are sampled from cluster-specific multivariate Gaussians; binary covariates are drawn as independent Bernoulli variables. The control outcome follows a nonlinear function of the covariates:

$$\mu^0(\mathbf{x}) = \sin(\pi x_1 x_2) + 0.2(x_3 - 0.5)^2 + \frac{\exp(x_4)}{1 + \exp(x_5)} + x_6^2 + 0.3x_7 + \log(1 + x_8 x_9) + 2(x_{10} - 0.5)^2 + x_{11} x_{12}$$

with additive Gaussian noise ($\sigma = 1$) for both y^0 and y^1 . Constant treatment effects are assigned per cluster: $\tau = (0.5, 5, -5, 0, 0)$, and the treated proportion is 0.5 (with a parallel dataset at 0.2).

Figure B.2 displays the true potential outcomes (y^0, y^1) for each individual, colored by ground-truth cluster membership. The dashed line represents the $y^1 = y^0$ diagonal (i.e., zero treatment effect). Clusters 2 (orange, $\tau = 5$) and 3 (green, $\tau = -5$) are clearly separated above and below the diagonal, respectively, reflecting their strong positive and negative treatment effects. In contrast, Clusters 1 (blue, $\tau = 0.5$), 4 (red, $\tau = 0$), and 5 (purple, $\tau = 0$) lie close to the diagonal, consistent with their near-null effects. This visualization highlights the challenge faced by causal clustering methods that rely solely on potential outcome vectors: Clusters 4 and 5 overlap substantially in (y^0, y^1) space despite being well-separated in covariate space, underscoring the advantage of BSCC in leveraging covariate information alongside treatment effect supervision.

We show the comparison results of our model to common supervised learning methods for the heterogeneous treatment effects listed in the main text. Since supervised learning methods, except subgroup analysis MOB, do not produce cluster labels, we further use GMM to cluster the estimated treatment effects to obtain cluster labels. We see that our BSCC performs the best on the simulated dataset in terms of the metrics. All other supervised learning methods tend to either underestimate or overestimate the treatment effects, resulting in larger errors. Some individuals are misclassified based on treatment effects only as shown in Figure 3. For subgroup analysis method MOB, it will learn more clusters than the ground truth due to the fashion of splitting one covariate at a time, also poor in capturing interactions between multiple covariates. Figure B.3 presents additional UMAP projections of covariate space colored by cluster assignments from IT, FINDIT, and OWE. IT identifies only 3 clusters, merging subgroups with distinct treatment effects. FINDIT assigns nearly all individuals to a single dominant cluster, consistent with its near-degenerate SATE range and high PEHE. OWE recovers 4 clusters but exhibits substantial misclassification across covariate regions, reflecting its limited ability to capture the underlying heterogeneity.

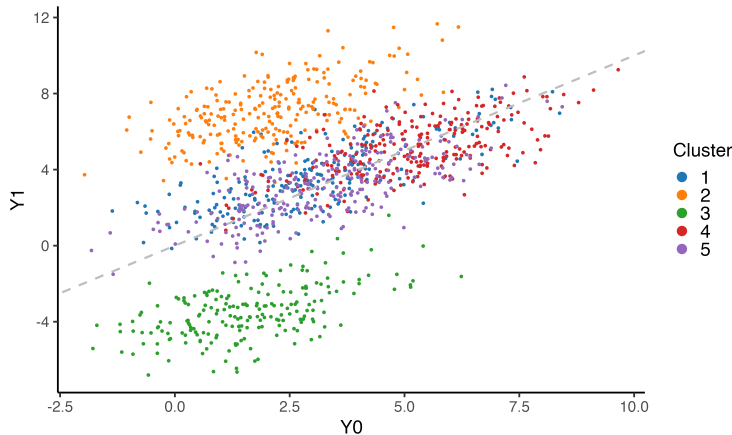


Figure B.2: True potential outcomes (y^0, y^1) for SIMULATION HTE, colored by ground-truth cluster membership. The dashed line indicates $y^1 = y^0$ (zero treatment effect).

B.3 Homogeneous and Null Treatment Effects Test.

We are clustering over covariates and treatment outcomes simultaneously. Thus, in the homogeneous and null treatment effects case, we can find clusters over covariates as a standard Bayesian mixture model will, but without differences in treatment effects, or we can find clusters with similar covariates but opposite treatment effects, as illustrated by the results in Table B.6. In the test set, however, these might lead to null treatment effects clusters with redundant or tiny clusters, showing some

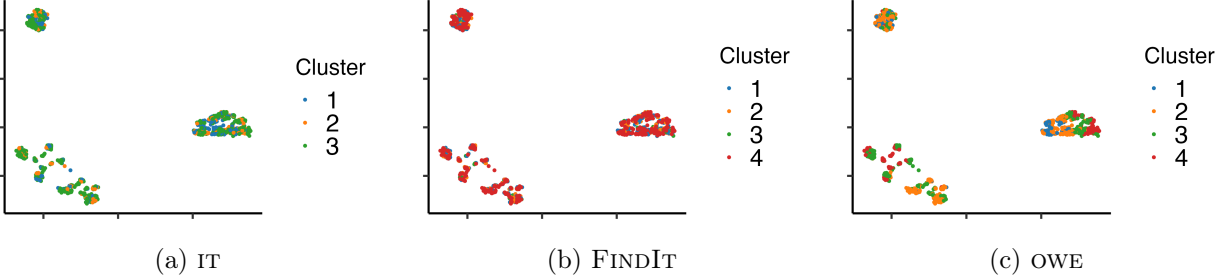


Figure B.3: UMAP projections of covariate space for SIMULATION HTE, colored by cluster assignments from **(a)** IT, **(b)** FINDIT, and **(c)** OWE.

Table B.4: Sensitivity Test of Prior SD of constant β_k on SIMULATION HTE.

β_k SD	ARI	Range of τ_k	PEHE
0.5	0.750	[-4.810 4.984]	0.847
1	0.733	[-4.766, 5.020]	0.943
5	0.733	[-4.750, 4.927]	0.944
10	0.732	[-4.841, 5.059]	0.983
100	0.739	[-4.812, 5.006]	0.987

Table B.5: Sensitivity Test of Prior Mean of constant β_k on SIMULATION HTE.

β_k Mean	ARI	Range of τ_k	PEHE
(0,0,0,0)	0.733	[-4.766, 5.020]	0.943
(0,0,-5,5)	0.751	[-4.790, 5.029]	0.885

inconsistency between training and test results. Only when we can choose the correct number of clusters by validation metrics to be 1 can we avoid the false positive discovery.

Table B.6: Test of Homogeneous and Null Treatment Effects on SIMULATION NULL. We have only one cluster of individuals with zero treatment effects.

K	Train RMSE of Control	Test RMSE of Control	Train PEHE	Test PEHE	Train Range of τ_k	Test Range of SATE
1	0.217	0.460	0.048	0.048	[0.048, 0.048]	[-0.057,-0.057]
2	0.210	0.460	0.386	0.382	[-0.347, 0.429]	[-0.172, -0.025]
3	0.201	0.529	0.386	0.268	[-0.550, 0.733]	[-6.29, -0.048]
4	0.203	0.524	0.368	0.223	[-0.694, 1.232]	[-0.138,0.029]
5	0.216	0.472	0.361	0.189	[-0.748, 1.240]	[-0.0224,-0.0215]

B.4 Posterior Distribution of Parameters

Denote the parameters for potential outcomes as $\theta^y = \{\sigma_0, \sigma_1, \{\mu_n^0\}_{n=1}^N, \phi = \{\alpha, \rho\}\}$ where α, ρ are only available for Gaussian kernel. Then the posterior of parameters $\Theta = \{\{\theta_k, \gamma_k, \beta_k\}_{k=1}^K, \theta^y, \pi\}$ is:

$$\begin{aligned}
 p(\Theta | \mathcal{D}) &\propto p(\mathcal{D} | \Theta)p(\Theta) \\
 &\propto \prod_{n=1}^N \left\{ p(a_n | \mathbf{x}_n) \sum_{k=1}^K \Pr(z_n = k) p(\mathbf{x}_n | z_n = k) p(y_n^{\text{obs}} | a_n, \mathbf{x}_n, z_n = k) \right\} p(\Theta) \\
 &\propto \prod_{n=1}^N \left\{ \sum_{k=1}^K \Pr(z_n = k) p(\mathbf{x}_n | z_n = k) p(y_n^{\text{obs}} | a_n, \mathbf{x}_n, z_n = k) \right\} p(\Theta) \\
 &\hspace{15em} (p(a_n | \mathbf{x}_n) \text{ is known under randomization}) \\
 &\propto \prod_{n=1}^N \left\{ \sum_{k=1}^K \pi_k p(\mathbf{x}_n | \theta_k) p(y_n^{\text{obs}} | a_n, \{\mu_n^0\}_{n=1}^N, \sigma_0, \sigma_1, \beta_k) \right\} p(\Theta)
 \end{aligned}$$

C Additional Real Application Results

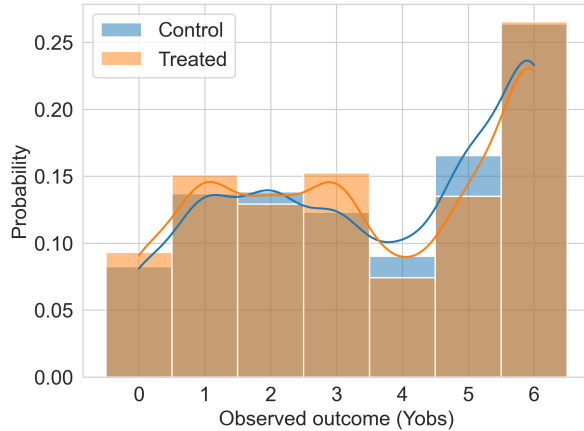


Figure C.4: IST-3 Data: Oxford Handicap Score (OHS) at 6 months outcome distributions for control and treated groups.

Figure C.4 shows the distribution of OHS outcomes for the IST-3 dataset. Table C.7 describes the covariates selected for the IST-3 dataset. Table C.10 and Table C.12 summarise the detailed statistics and resulting values for the training set corresponding to the cluster means radar chart and OR plots in the main content, while Table C.11 and Table C.13 summarise those for the test set. Table C.14 summarises the contingency table of clustering given by GMM. Table C.9 presents the performance of BSCC against other supervised learning models on the IST-3 dataset. We see that despite slightly smaller test policy risk (max difference around 0.03, which is about 40 individuals' decisions due to uncertainty) of supervised learning methods, all the supervised learning models yield unstable subgroups in terms of log OR (SATE) based solely on treatment effects, as shown by the train and test range of SATE. The corresponding radar charts and OR plots are shown in Figure C.6, Figure C.7, Figure C.8 and Figure C.9. For the subgroup analysis method MOB in Figure C.10,

we see that it is relatively consistent in training and test results, although no significant clusters are found. However, it obtained four clusters based on the splitting covariates "NIHSS" and "age" only, which ignored important covariates such as stroke subtypes found by BSCC.

Table C.7: List of Covariates Used for the IST-3 Dataset.

Description of Covariate	Feature Type
Age	Continuous
Delay Time from onset of stroke symptoms to randomisation (h)	Continuous
Systolic blood pressure (mmHg)	Continuous
Diastolic blood pressure (mmHg)	Continuous
Glucose (mmol/L)	Continuous
NIHSS (Stroke Score at randomisation)	Continuous
Sex	Binary
Treatment with antiplatelet drugs in previous 48 h?	Binary
Atrial fibrillation?	Binary
Acute ischaemic change on randomisation scan according to expert panel?	Binary
Clinician’s assessment of recent ischaemic change at randomisation	Categorical (No, Possible, Definite)
Stroke syndrome (type)	Categorical (TACI, PACI, LACI, POCI, Other)

Table C.8: The Evaluation Metrics for Selecting the Number of Clusters of the IST-3 Dataset.

No. Clusters	Test Acc. of Control Outcome	Test Policy Risk
$K = 2$	0.754	0.648
$K = 3$	0.770	0.644
$K = 4$	0.762	0.644

Table C.9: A Summary of Model Performance for Different Supervised Learning Models on IST-3 Data.

Model Case	Train Range of SATE	Test Range of SATE	Test Policy Risk
BSCC	[-0.273, 0.658]	[-0.243, 0.501]	0.644
CF	[-1.942, 2.079]	[-0.249, 0.172]	0.616
BART	[-0.058, 2.521]	[-0.204, 0.636]	0.632
DR-LEARNER	[-3.563, 4.348]	[-0.165, 0.071]	0.621
R-LEARNER	[-1.941, 2.603]	[-0.270, 0.096]	0.618
MOB	[-0.621, 0.416]	[-0.724, 0.355]	0.638

Table C.10: IST-3: Summary Statistics (Min/Max/Mean) of Covariates by Clusters for Training Set (BSCC).

	Max	Min	Popu	Cluster1	Cluster2	Cluster3
Age	89.84	66.08	78.07	73.42	81.68	80.54
Delay2Rand	4.37	3.14	3.78	3.98	3.49	3.68
SBloodPres	171.79	139.70	155.27	155.22	155.38	156.17
DBloodPres	92.70	71.42	81.61	84.28	79.36	82.03
Glucose	8.06	6.30	7.29	7.32	7.32	7.00
NIHSS	19.50	7.31	12.25	8.12	17.73	12.22
Gender	1.00	0.00	0.53	0.42	0.54	0.61
AntiPlat	1.00	0.00	0.51	0.51	0.52	0.51
AtrialFib	1.00	0.00	0.32	0.25	0.38	0.32
VisInfarct	1.00	0.00	0.36	0.28	0.49	0.36
RecInfarct_Definite	1.00	0.00	0.16	0.09	0.24	0.21
RecInfarct_No	1.00	0.00	0.60	0.67	0.50	0.60
RecInfarct_Possible	1.00	0.00	0.24	0.23	0.31	0.24
StrokeType_LACI	1.00	0.00	0.12	0.21	0.01	0.08
StrokeType_Other	1.00	0.00	0.00	0.00	0.00	0.01
StrokeType_PACI	1.00	0.00	0.37	0.62	0.00	0.36
StrokeType_POCI	1.00	0.00	0.08	0.12	0.00	0.07
StrokeType_TACI	1.00	0.00	0.42	0.01	1.00	0.43

Table C.11: IST-3: Summary Statistics (Min/Max/Mean) of Covariates by Clusters for Test Set (BSCC).

	Max	Min	Popu	Cluster1	Cluster2	Cluster3
Age	88.48	67.16	77.32	74.62	80.44	78.47
Delay2Rand	4.52	3.34	3.93	4.10	3.71	3.88
SBloodPres	171.26	138.54	155.09	155.69	153.93	155.61
DBloodPres	91.99	72.21	82.26	83.63	80.23	82.42
Glucose	8.07	6.30	7.23	7.25	7.34	7.00
NIHSS	18.99	7.26	12.12	8.06	17.26	13.08
Gender	1.00	0.00	0.52	0.47	0.59	0.52
AntiPlat	1.00	0.00	0.52	0.52	0.53	0.49
AtrialFib	1.00	0.00	0.29	0.20	0.39	0.34
VisInfarct	1.00	0.00	0.37	0.26	0.52	0.40
RecInfarct_Definite	1.00	0.00	0.18	0.12	0.26	0.20
RecInfarct_No	1.00	0.00	0.59	0.69	0.48	0.56
RecInfarct_Possible	1.00	0.00	0.23	0.19	0.27	0.23
StrokeType_LACI	1.00	0.00	0.10	0.18	0.00	0.09
StrokeType_Other	1.00	0.00	0.00	0.00	0.00	0.00
StrokeType_PACI	1.00	0.00	0.39	0.66	0.00	0.40
StrokeType_POCI	1.00	0.00	0.09	0.15	0.00	0.08
StrokeType_TACI	1.00	0.00	0.42	0.00	1.00	0.43

Table C.12: IST-3: Contingency Table of Clusters for Training Set (BSCC).

Cluster	Group	Mortality	Alive	Mortality Prop.
Cluster1	Treated	53	265	16.7%
Cluster1	Control	43	280	13.3%
Cluster2	Treated	92	133	40.9%
Cluster2	Control	100	110	47.6%
Cluster3	Treated	49	86	36.3%
Cluster3	Control	36	122	22.8%

Table C.13: IST-3: Contingency Table of Clusters for Test Set (BSCC).

Cluster	Group	Mortality	Alive	Mortality Prop.
Cluster1	Treated	45	287	13.6%
Cluster1	Control	51	255	16.7%
Cluster2	Treated	74	131	36.1%
Cluster2	Control	102	143	41.6%
Cluster3	Treated	49	100	32.9%
Cluster3	Control	30	101	22.9%

Table C.14: IST-3: Contingency Table of Clusters for GMM.

Cluster	Group	Mortality	Alive	Mortality Prop.
Cluster1	Treated	244	276	46.9%
Cluster1	Control	248	277	47.2%
Cluster2	Treated	81	488	14.2%
Cluster2	Control	81	489	14.2%
Cluster3	Treated	37	238	13.5%
Cluster3	Control	33	245	11.9%

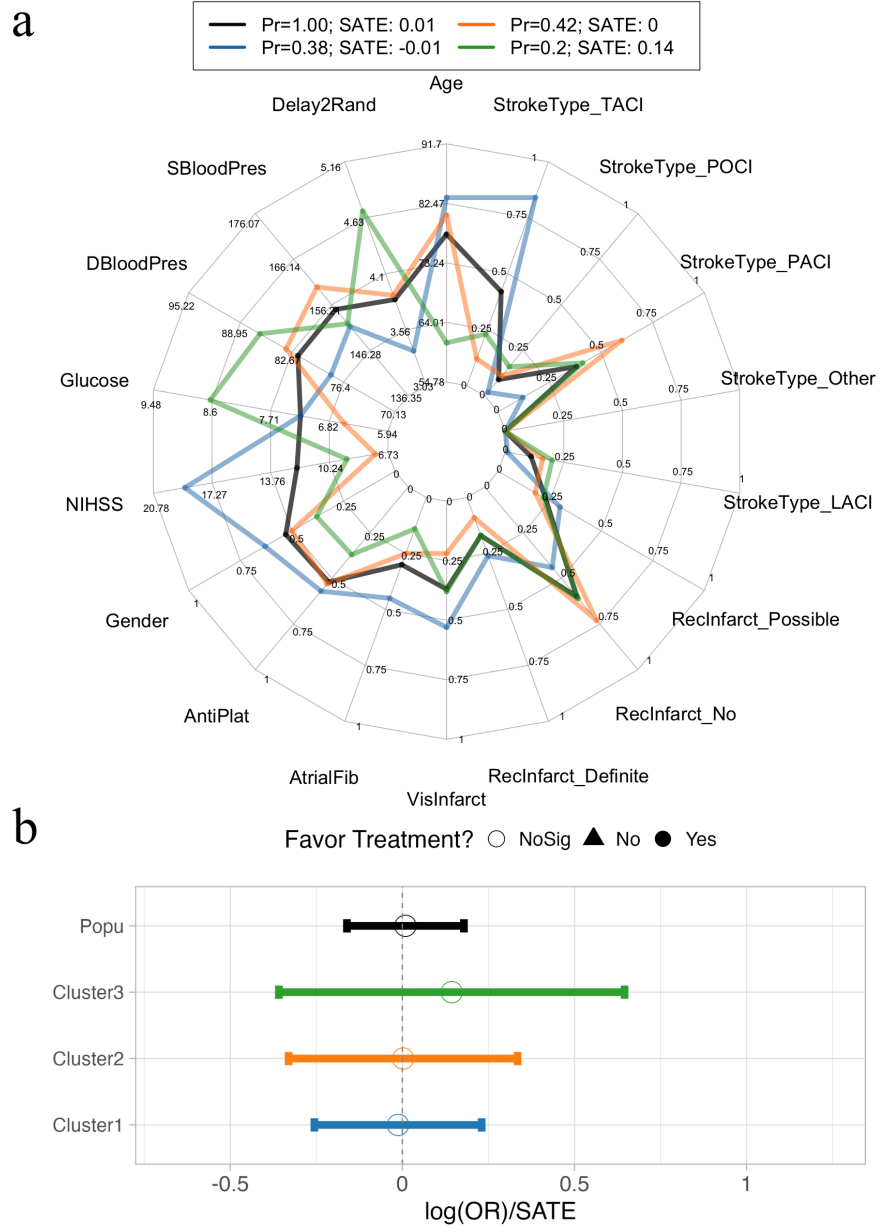
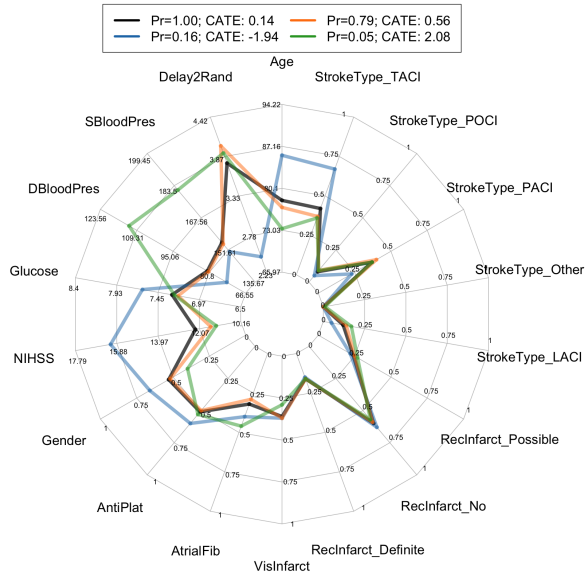
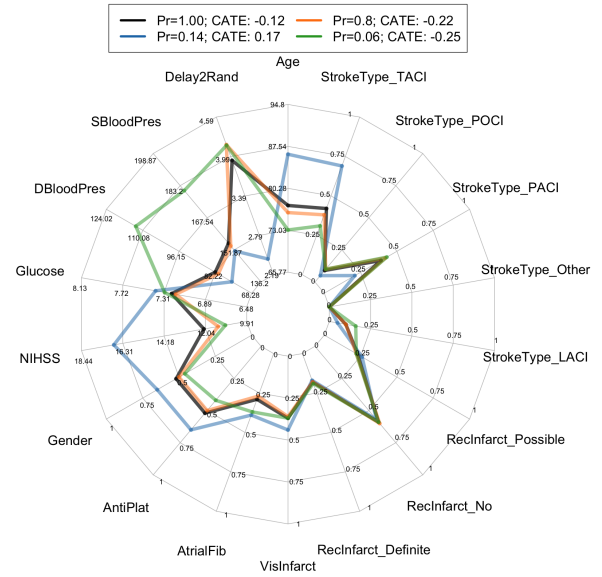


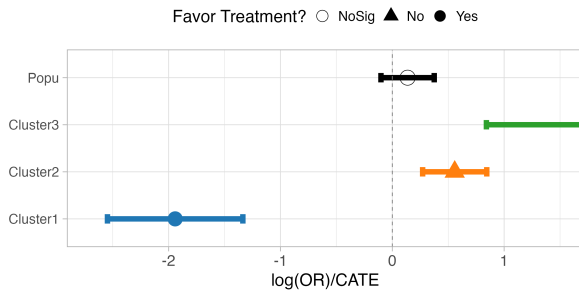
Figure C.5: GMM on IST-3 Dataset: (a) The estimated cluster means and (b) ORs with 95% CIs (log scale) when $K = 3$.



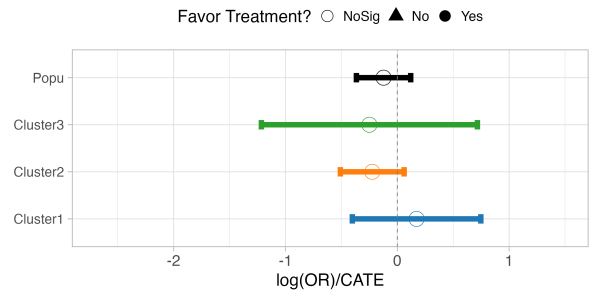
(a) Estimated cluster means on train set



(b) Empirical cluster means on test set

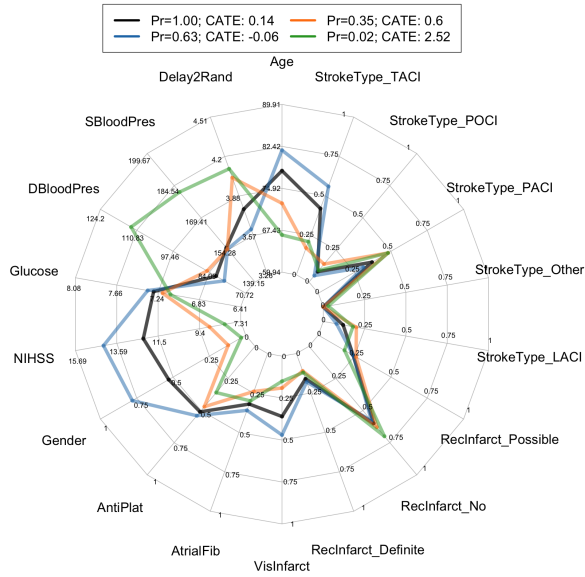


(c) ORs with 95% CIs for train set

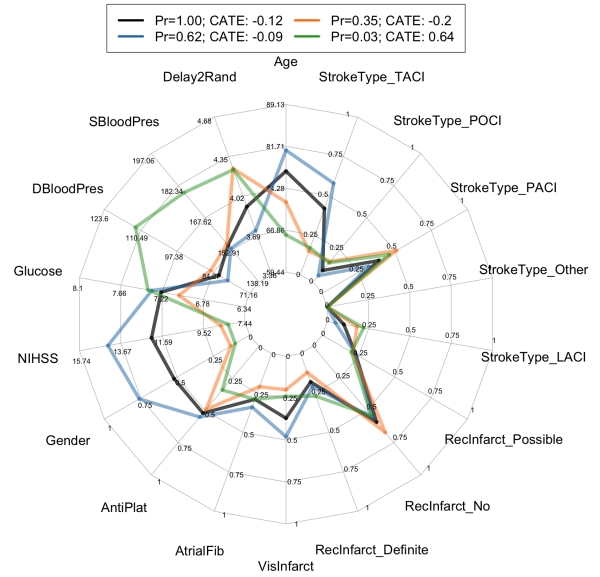


(d) ORs with 95% CIs for test set

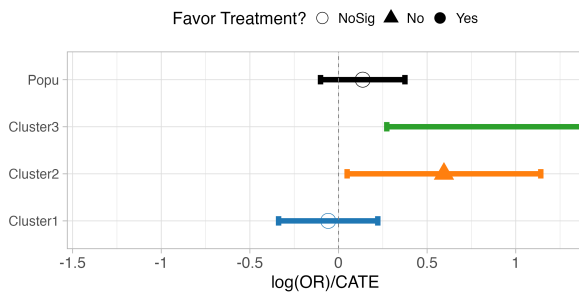
Figure C.6: CF on IST-3 Dataset.



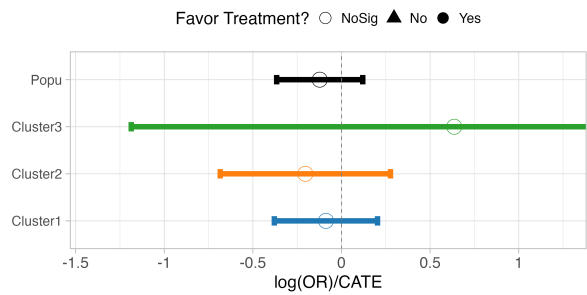
(a) Estimated cluster means on train set



(b) Empirical cluster means on test set

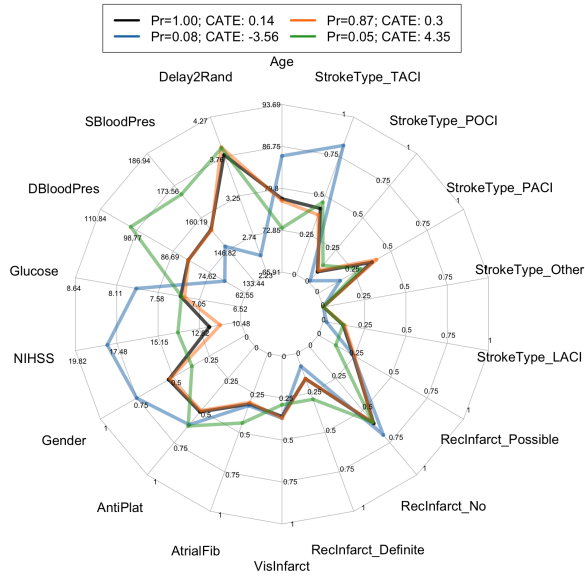


(c) ORs with 95% CIs for train set

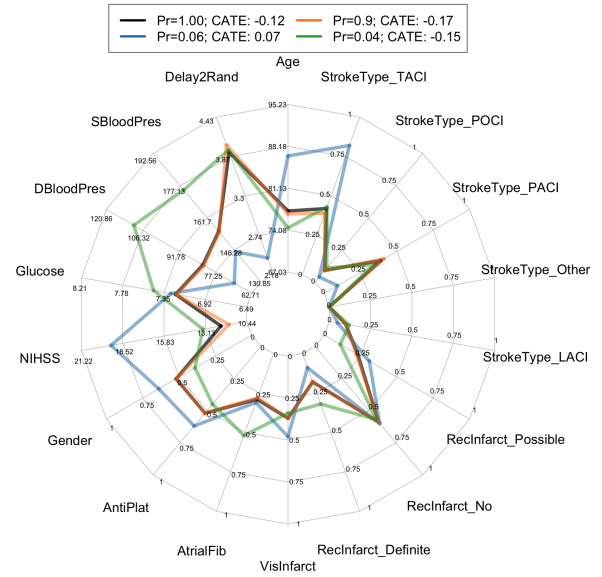


(d) ORs with 95% CIs for test set

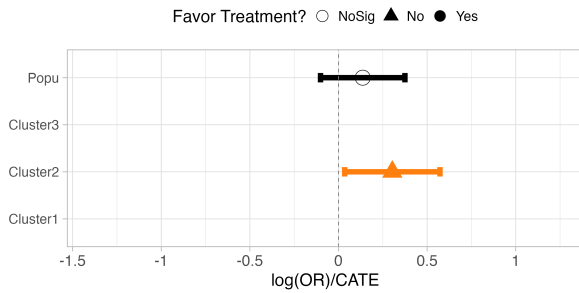
Figure C.7: BART on IST-3 Dataset.



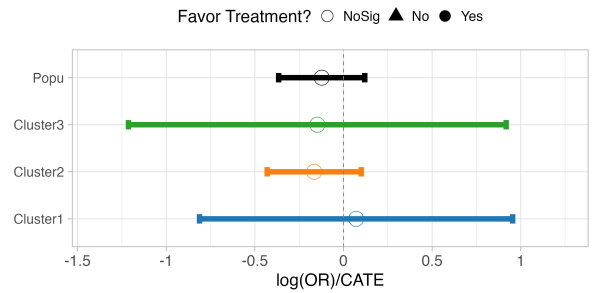
(a) Estimated cluster means on train set



(b) Empirical cluster means on test set

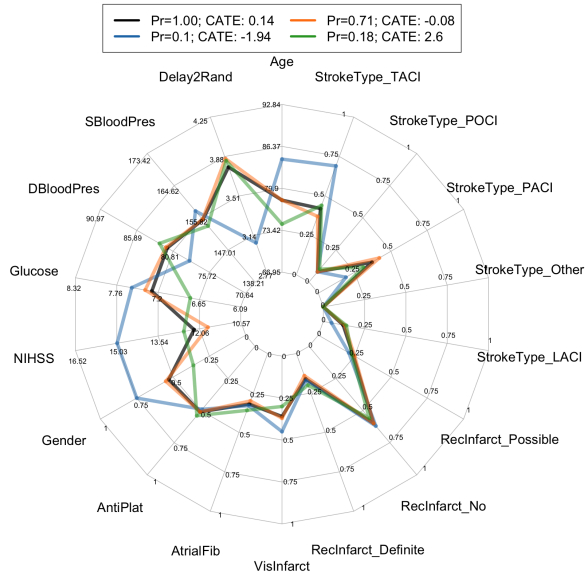


(c) ORs with 95% CIs for train set

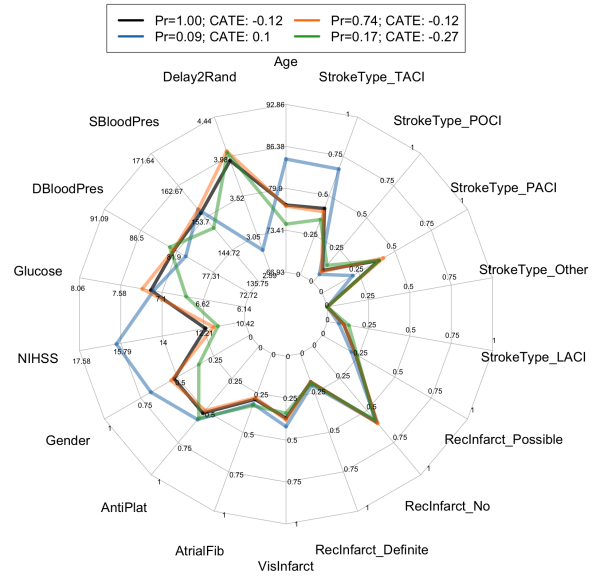


(d) ORs with 95% CIs for test set

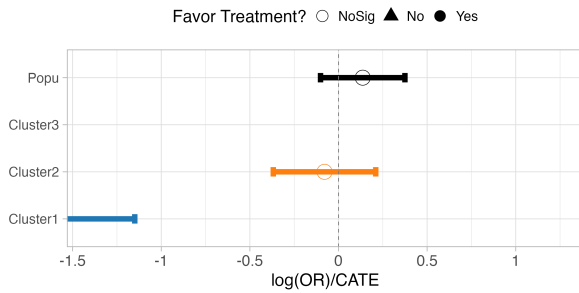
Figure C.8: DR-LEARNER on IST-3 Dataset.



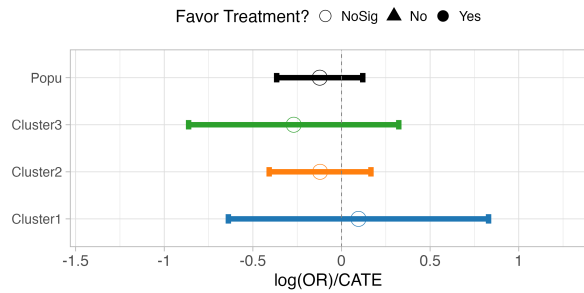
(a) Estimated cluster means on train set



(b) Empirical cluster means on test set

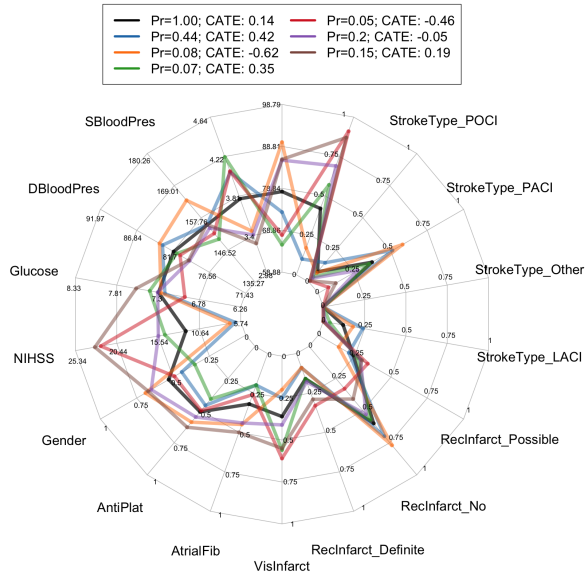


(c) ORs with 95% CIs for train set

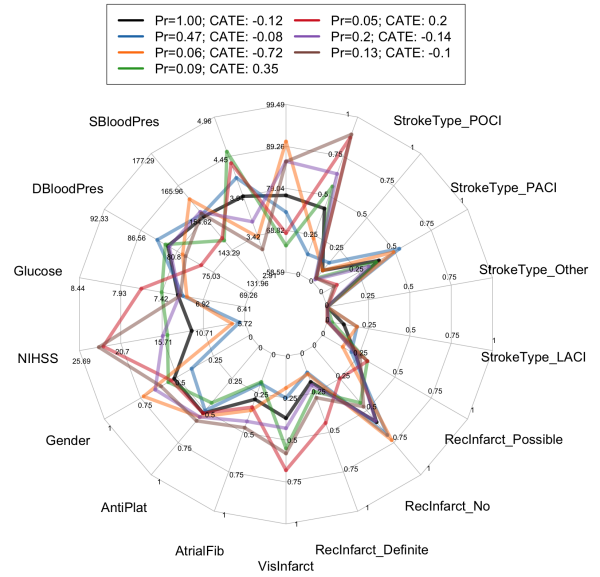


(d) ORs with 95% CIs for test set

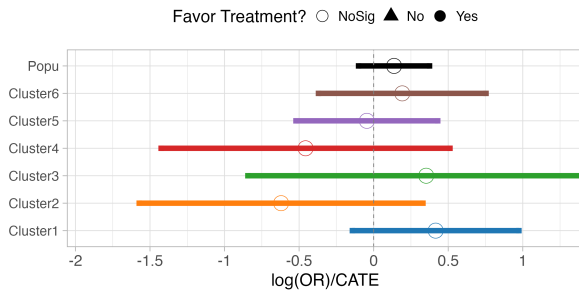
Figure C.9: R-LEARNER on IST-3 Dataset.



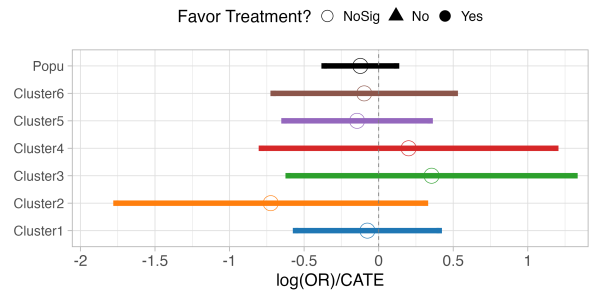
(a) Estimated cluster means on train set



(b) Empirical cluster means on test set



(c) ORs with 95% CIs for train set



(d) ORs with 95% CIs for test set

Figure C.10: MOB on IST-3 Dataset.